

# Photochemistry of solid C<sub>60</sub> with tunable infrared radiation

G. von Helden, I. Holleman, M. Putter, G. Meijer

Dept. of Molecular and Laser Physics, University of Nijmegen, Toernooiveld, 6525 ED Nijmegen, The Netherlands

Received: 14 April 1998/Accepted: 22 April 1998

**Abstract.** The interaction of solid C<sub>60</sub> with trains of picosecond infrared (IR) pulses, tuned over the 8–15 μm range, is studied. At some specific wavelengths, white-light emission as well as ejection of ionic species from the solid is observed. The spectral characteristics of the white-light emission resemble those of a black body. The mass distribution of the ejected ionic species shows substantial amounts of C<sub>60</sub> coalescence products. Unexpectedly, all these processes only occur at wavelengths where solid C<sub>60</sub> is relatively transparent. No white-light emission nor ejection of ionic species is observed when being resonant with an IR-allowed transition of C<sub>60</sub>. It is concluded that regular C<sub>60</sub> is not the chromophore for the observed processes, and that sequential absorption of single photons by a strong absorber that is dilute in the crystal takes place. Plausible chromophores are sites that are intercalated with alkali metals. Accumulation of energy at these sites leads to fullerene coalescence in the solid, ion ejection, and white-light emission, ultimately resulting in the destruction of the C<sub>60</sub> molecules.

**PACS:** 36; 79.60; 81.40

C<sub>60</sub> is a molecule with many remarkable properties. Its high molecular symmetry makes C<sub>60</sub> perhaps the largest molecule that can be understood in detail. Over the last years, solid-state properties of C<sub>60</sub> have attracted a lot of attention [1]. Its strong intramolecular and weak intermolecular binding makes solid C<sub>60</sub> an ideal model system for a molecular crystal, and enables facile intercalation with a variety of species. Solid C<sub>60</sub> can be efficiently intercalated with metal atoms resulting in a pronounced modification of its electronic properties. As one of the most spectacular results, A<sub>3</sub>C<sub>60</sub> (A=K, Rb, Cs) intercalation compounds are shown to have a superconducting phase [2], and A<sub>1</sub>C<sub>60</sub> [3] compounds can polymerize and have metallic phases [4].

As a consequence of the facile intercalation, one has to consider the possibility of impurities when analyzing experimental results on solid C<sub>60</sub>. In addition, although C<sub>60</sub> is a fairly stable molecule, solid C<sub>60</sub> can be chemically modified

when irradiated by light of an intense enough laser and complications can arise from (reversible) photopolymerisation [5] or photo-assisted oxidation of C<sub>60</sub> [6].

Some potentially interesting properties of solid C<sub>60</sub> are presently not well understood. Among these is the intense ‘white-light emission’ first observed by Feldmann and coworkers [7] and later reported upon by Roth and coworkers in a series of similar papers [8–10]. This white-light emission is observed when exciting crystalline C<sub>60</sub> by visible or near-infrared ps laser light [7–9] or by electric current (electroluminescence) [10]. Recently, it was pointed out that, in the case of electroluminescence, impurities in the solid are important for the initiation of white-light emission and that C<sub>60</sub> irreversibly decomposes in this process [11].

In this article we present results on the processes that occur when solid C<sub>60</sub> is irradiated by a train of intense ps pulses of infrared (IR) light. At specific wavelengths, white-light emission is observed, and its spectral characteristics are determined. The emission intensity is monitored as a function of IR laser fluence and wavelength as well as of sample condition. When C<sub>60</sub> single crystals are illuminated under high-vacuum conditions the ejection of C<sub>60</sub><sup>+</sup> as well as other ions is observed, indicating that the IR laser triggers a high-energy process. A plausible mechanism leading to the white-light emission and the ejection of ions is presented, which has devastating implications for the anticipated ‘device performance’ [10].

## 1 Experimental

The experiments have been performed at the FELIX user facility (‘Free Electron Laser for Infrared eXperiments’) in Nieuwegein, The Netherlands [12,13]. This laser produces IR radiation that is continuously tunable over the 100–2000 cm<sup>-1</sup> range with a typical bandwidth of 0.5% of the central frequency (5 cm<sup>-1</sup> at 10 μm). The light output consists of macropulses of about 5 μs duration containing up to 50 mJ of energy, although in all experiments reported here macropulse energies of only 1–5 mJ are used. Each macropulse consists of a train of micropulses that are approxi-

mately 1 ps long and 1 ns apart. The macropulse repetition rate is 5 Hz. The IR beam is about 3 mm in diameter, and no focusing is applied in any of the experiments. The corresponding peak powers are  $\approx 3\text{--}15\text{ MW/cm}^2$ .

Three different kinds of  $\text{C}_{60}$  sample, thin films, polycrystalline powder, or single crystals are used in these experiments. The starting material for all these samples is polycrystalline  $\text{C}_{60}$  powder with a stated purity of  $\geq 99.9\%$  (Hoechst 'Super gold grade'  $\text{C}_{60}$ ) which is heated under vacuum for a prolonged period of time to remove residual solvents.  $\text{C}_{60}$  thin films are obtained by sublimation of this starting material onto an IR-transparent substrate (KBr or ZnSe).  $\text{C}_{60}$  single crystals are grown from re-sublimed  $\text{C}_{60}$  powder in an evacuated and sealed quartz tube. The detailed procedure for growing  $\text{C}_{60}$  crystals has been published elsewhere [14].

In the optical emission studies, the sample is located in a nitrogen atmosphere, and rests on an ceramic plate. A small hole in this plate allows the simultaneous measurement of transmission spectra of  $\text{C}_{60}$  samples using a pyrodetector. Emitted light is either collected through an IR microscope with reflective optics onto a red-sensitive photomultiplier tube (PMT, RCA C31034-02), or measured directly with a photodiode (EG&G, FND-100Q). In one experiment, the light is measured simultaneously with the photodiode and with a MCT (Graseby, HCT-21-C) detector. In front of the MCT detector, a sapphire and a germanium window are placed, transmitting only light in the wavelength range between  $2\text{ }\mu\text{m}$  and  $6\text{ }\mu\text{m}$ . For spectral analysis of the emitted light a monochromator together with the above-mentioned PMT is used for the visible region, and a FTIR spectrometer (Bruker IFS 66v) equipped with a standard IR beamsplitter (Ge-KBr) and a DTGS detector is used for the infrared region.

To study the laser-induced ejection of ions from solid  $\text{C}_{60}$  samples, experiments are performed under high-vacuum conditions. The apparatus consists of a turbo-pumped vacuum system (pressure in the  $10^{-7}\text{--}10^{-8}$  Torr range) containing a short time-of-flight (TOF) mass spectrometer. The  $\text{C}_{60}$  crystal rests on a gold-coated copper disc that is mounted on a temperature-variable manipulator arm. Prior to the experiment, the crystals are heated to 500 K to remove surface contaminants and/or oxides. The target holder is flush with the lowest TOF plate, which is at ground potential. The second plate is pulsed to an intermediate negative high-voltage level while the third plate together with the flight tube are on the final (negative) high-voltage level. Ions are then detected on a dual micro-channel plate (MCP) detector. The signal is amplified, recorded on a digital oscilloscope, and transferred to a PC for further analysis.

## 2 Results

### 2.1 White light emission

An intense pulsed white-light emission is observed from the  $\text{C}_{60}$  target, when illuminating it with unfocused IR light of specific wavelengths and sufficient power. In Fig. 1a the time-integrated white-light emission intensity of a thick  $\text{C}_{60}$  crystal, as measured with the silicon photodiode, is shown as a function of the frequency of the excitation laser. Clear peaks

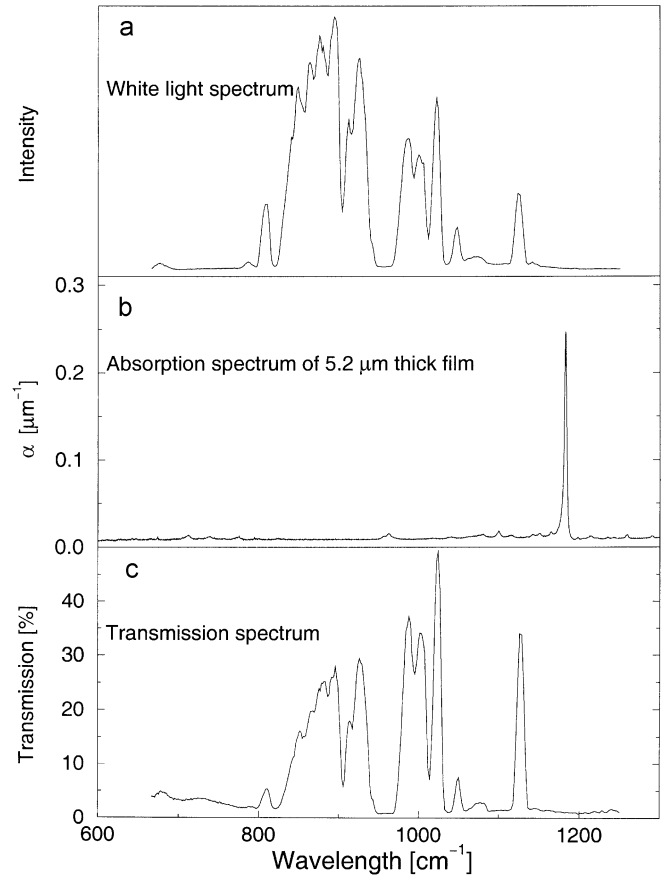


**Fig. 1.** **a** Time-integrated emission intensity of a thick  $\text{C}_{60}$  crystal as a function of the frequency of the excitation laser. **b** Absorption spectrum of a  $5.2\text{-}\mu\text{m}$ -thick film of  $\text{C}_{60}$  measured in an FTIR spectrometer. **c** Transmitted FELIX light through the thick  $\text{C}_{60}$  crystal, measured simultaneously with **a**

are observed, separated by regions of no intensity. For comparison, the absorption spectrum of a  $5.2\text{-}\mu\text{m}$ -thick film of  $\text{C}_{60}$  is shown in Fig. 1b. No white-light emission is observed when the IR laser is resonant with IR-allowed  $\text{C}_{60}$  transitions. In Fig. 1c the transmission spectrum through the same crystal, measured simultaneously with the emission spectrum, is shown. The white-light emission spectrum and the transmission spectrum are very similar.

This similarity is consistent with another observation that, at the start of a new experiment, the white-light emission predominately originates from regions near the bottom of the crystal. When such a crystal is then turned around, after some exposure time to the IR laser, emission is also observed from localized spots on the top of the crystal. When the emission occurs from the top of the crystal, white-light emission is observed to be more or less independent of the excitation wavelength. White-light emission can also be observed from other  $\text{C}_{60}$  samples, such as polycrystalline  $\text{C}_{60}$  powder and thin films. In many instances it turned out to be necessary to fire the laser onto the target for some time before emission is initiated. Also in these cases, the excitation spectra are structureless and show no correlation with the  $\text{C}_{60}$  absorption spectrum. Whereas emission from thick crystals remains stable for days, powders and thin films slowly stop emitting light after several minutes to hours. For all samples studied, a strong dependence of the white-light emission intensity on

the intensity of the IR excitation light is observed; the time-integrated white-light emission intensity as detected with the photodiode scales roughly with the intensity of the IR excitation light to the 6th–10th power. However, as discussed below, this apparent power dependence does not give a direct physical meaningful insight into the process when only the short-wavelength tail of a blackbody emission curve is detected.

In Fig. 2, the time-integrated dispersed emission spectrum of a  $C_{60}$  crystal is shown for a fixed value of the excitation wavelength ( $11.2\ \mu\text{m}$ ) and fluence. The visible part of the spectrum is recorded by passing the light through a monochromator and measuring the intensity of the light by a red-sensitive PMT. The near-infrared part of the spectrum is recorded with the FTIR spectrometer and the DTGS detector. Both spectra are corrected for the overall wavelength-dependent detection efficiency of the corresponding spectrometers. Since neither of the two spectra are collected on an absolute scale, and as both spectra unfortunately do not overlap, an a priori unknown scaling factor is connecting the two. In Fig. 2, this scaling factor is chosen such as to suit the eye. Shown as dashed lines in the figure are blackbody emission curves for temperatures of 2000 K, 3000 K, and 4000 K. The experimental curve is closest to that of a blackbody at a temperature of 3000 K. The experimental curve is somewhat narrower than a calculated blackbody curve, for which several effects could be responsible. First, a blackbody emission spectrum is only observed when the sample is at thermal equilibrium and when the density of states is high. Although the density of states in our sample is certainly sufficiently high, it is not necessarily clear that the state distribution at the emitting sites can be described by a Boltzmann distribution at all. Second, self-absorption of  $C_{60}$  could be of importance, reducing the observed intensity of light emanating from the sample

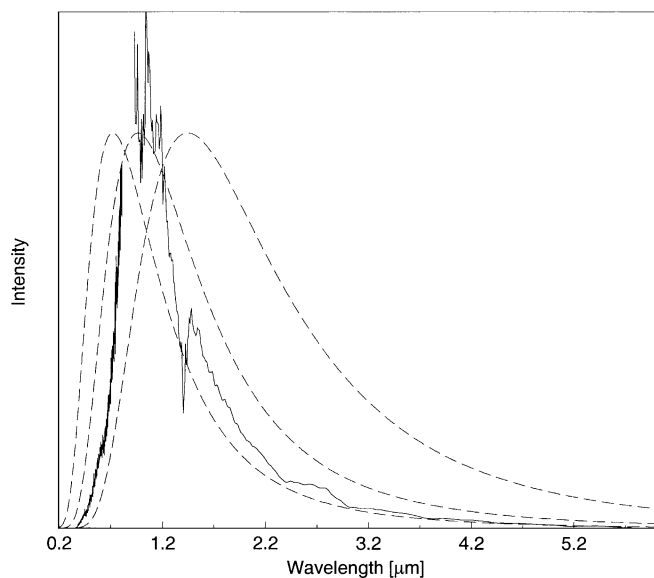


**Fig. 2.** Time-integrated dispersed emission spectrum of a  $C_{60}$  single crystal excited by a train of ps IR pulses at  $890\ \text{cm}^{-1}$ . The visible part of the spectrum is measured with a monochromator and the near-infrared part is measured with the FTIR spectrometer. Both spectra are corrected for the wavelength-dependent detection sensitivity of the spectrometers. The dashed lines are blackbody curves for temperatures of 4000 K, 3000 K, and 2000 K

in the short-wavelength region of the spectrum [15]; after all, a  $\mu\text{m}$ -thick film of  $C_{60}$  already appears brownish to black to the eye [16]. In this case, the true maximum of the emission curve would lie further in the short-wavelength range and the blackbody temperature would be closer to 4000 K.

Furthermore, it should be noted that the spectrum shown in Fig. 2 is recorded by time-integrating the emitted light intensity. Since the corresponding ‘temperature’ of the white light will change continuously from room temperature to a high temperature and back, the interpretation of the data in terms of a single ‘temperature’ might be problematic. As the emissivity of a blackbody is highly nonlinear with respect to temperature, it is expected that the observed curve is selectively representative for the highest temperatures.

To elucidate further the processes involved, the time structure of the emitted light intensity from a  $C_{60}$  single crystal excited at  $11.2\ \mu\text{m}$  is examined. For this, two different detectors are employed: a Si photodiode that is sensitive throughout the visible range of the spectrum up to about  $1.1\ \mu\text{m}$  and a MCT detector with a sapphire and a germanium window in front, so that it is sensitive in the IR, between 2 and  $6\ \mu\text{m}$ . Their traces are shown in Fig. 3a. The corresponding envelope over the FELIX micropulses is shown in the lower part of this figure. It should be noted that both detectors and their corresponding amplifiers are fast enough so that on the time scale in Fig. 3, their time constant does not influence the shape of the curves. The data shown in Fig. 3a clearly shows that the curves from the Si and MCT detector are different. Both curves rise steeply in the beginning and then decay almost exponentially. However, the trace from the MCT detector starts earlier, rises less steeply and then decays much more slowly than the trace from the Si photodiode. It is therefore evident that the spectral distribution of the emission changes in time, since otherwise their shapes would be the same. It is therefore useless to try to extract a ‘power dependence’ from the rising part or a ‘lifetime’ from the falling part and the spectral

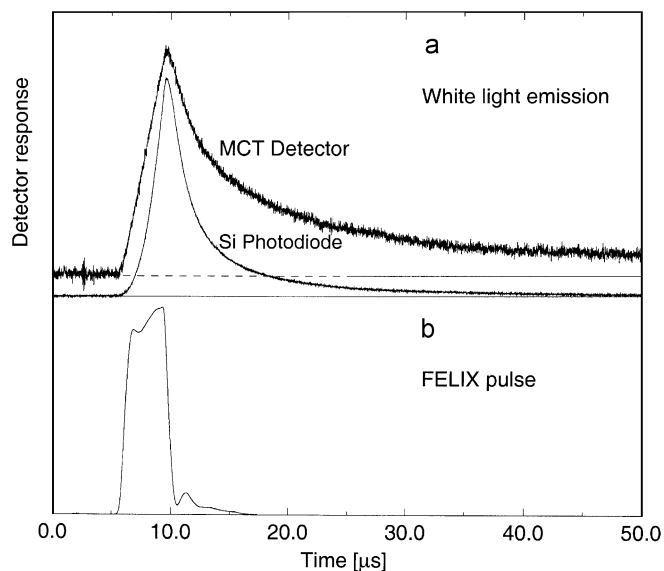


**Fig. 3.** **a** Time structure of the white-light emission intensity from a  $C_{60}$  single crystal, irradiated with a train of ps IR ( $11.2\ \mu\text{m}$ ) pulses, as detected with the photodiode and the IR-sensitive MCT detector. Their corresponding baselines are shown as horizontal lines. **b** Envelope of the micropulses used in recording the data displayed in **a**

emission characteristics of the sample as well as the spectral response of the detection system have to be taken into account before useful information on the underlying physical process can be extracted.

## 2.2 Ion ejection

In Fig. 4 we show a mass spectrum of the positively charged ions ejected from a  $C_{60}$  crystal when being illuminated with unfocused IR light at  $890\text{ cm}^{-1}$ . For these measurements, the region between the two lower TOF plates is initially field-free and pulsed to the acceleration field  $20\text{ }\mu\text{s}$  after the FELIX macropulse. This allows hot ejected fullerenes to auto-ionize [17, 18] and to drift towards the center between the lower two electrodes. The mass spectrum is dominated by an intense  $C_{60}^+$  peak, and almost no direct fragmentation products of  $C_{60}$  are observed. The only additional peaks at low masses are found at  $m/z$  values of 39 and 41, in an approximate 20:1 ratio, and are attributed to potassium since both their position and relative intensity match that of potassium in its natural isotope abundance. At masses higher than that of  $C_{60}^+$ , two groups of peaks are seen, as shown enlarged in the inset of the figure. The first group is rather symmetrically distributed around  $C_{122}^+$  while the other group is centered around a mass slightly higher than that of  $C_{180}^+$ . Individual peaks are separated by 24 amu, the mass of a  $C_2$  unit. Similar coalescence mass spectra, obtained by shining UV/VIS lasers on solid  $C_{60}$  targets have been reported by others [19]. In all these spectra, the distributions are different from the one reported here. The distributions are peaked below  $C_{120}^+$  and  $C_{180}^+$  and are skewed towards lower masses. Mechanisms of fullerene coalescence in the gas phase have been put forward to explain these observations [19].

The wavelength dependence of fullerene ion intensity is very similar to the dependence of the white-light emission intensity on excitation wavelength. Also in this case, no ions

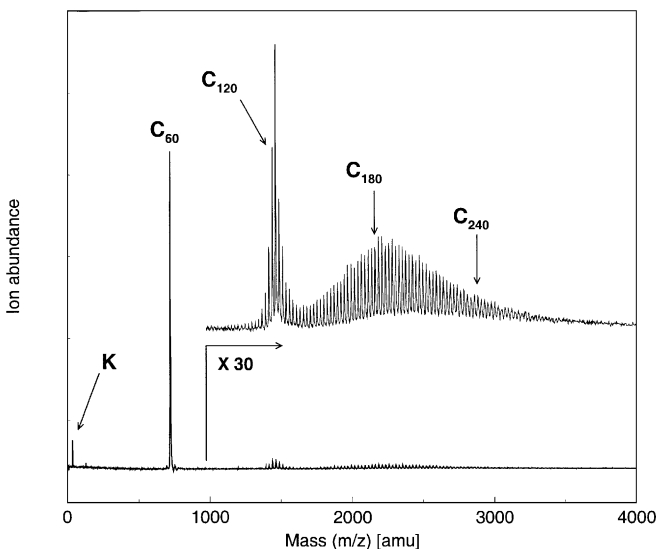


**Fig. 4.** Time-of-flight (TOF) mass spectrum of positively charged ions ejected from a  $C_{60}$  crystal. The unfocused IR laser is set at  $11.2\text{ }\mu\text{m}$ , at one of the peaks of the white-light emission spectrum (see Fig. 1). Apart from a large  $C_{60}^+$  signal, peaks resulting from fullerene coalescence processes are observed. At low masses, ion signal from potassium is observed

are ejected at wavelengths where  $C_{60}$  strongly absorbs the IR light. The generation of  $C_{60}^+$  using the IR laser appears to be a strongly nonlinear process, i.e. small changes in laser power result in large changes in ion signal. Again, the observed power dependence is difficult to interpret, however, and is not straightforwardly connected to the number of photons involved in some bottleneck step, for instance.

## 3 Discussion

White-light emission with a similar temporal profile to that shown in Fig. 2 is also observed when the FELIX beam impinges on 'black' surfaces such as graphite or black paint. The intensity of this emitted light, however, is at least an order of magnitude weaker than the intensity of the white-light emission from  $C_{60}$ . Furthermore, it should be emphasized that, although crystalline  $C_{60}$  appears 'black', it is best considered an IR-transparent material, especially at wavelengths where the most intense white-light emission and ion ejection occurs. In the IR-wavelength range used in this study, the  $1/e$  penetration depth ranges from  $4\text{ }\mu\text{m}$  on the resonance at  $1183\text{ cm}^{-1}$  to millimeters off resonance (see Fig. 1). This should be compared to sub- $\mu\text{m}$  penetration depths of IR light for graphite or black paint, resulting in absorbed energies per unit volume that are many orders of magnitude higher than in the  $C_{60}$  samples.

White-light emission from  $C_{60}$  material upon excitation with high-power lasers, was first reported by Feldmann et al. [7] and subsequently explored by Roth and coworkers [8, 9] resulting in a series of papers. In one of their more recent papers, it is assumed that, although details of the process leading to the observed light emission after excitation with ps laser pulses at 585 nm and 805 nm are still not understood, 'the increasing interaction between adjacent excitations at high excitation densities... leads to a comparable self-stabilization of the excited states and the emergence of new decay channels with different recombination mechanisms' [9].

The interpretation of the white-light emission process is largely based on the spectral characteristics of the observed emission together with the observed time and power dependence of this emission [7–9]. The reported emission spectra [8, 9] show a sharp cutoff towards long wavelengths at about 1100 nm. Instead, we observe emission that resembles that of a blackbody, extending far into the infrared. It has been pointed out by Palstra and coworkers [11] that in the case of electroluminescence of  $C_{60}$ , the reported cutoff at long wavelengths is actually due to the loss of sensitivity of silicon photodiode-based detectors, which was apparently not corrected for in the earlier work [7–10]; the actual emission spectrum in electroluminescence follows a blackbody curve with high emission intensity in the IR as well [11]. We are therefore led to assume that the white-light emission spectra reported to date are not corrected for the wavelength dependence of the detection system either. The spectral characteristics of the white-light emission are crucial for a correct interpretation of the observed time and power dependence of the emission intensity. Largely different interpretations can be given to these data, depending on whether a single state or a thermal distribution of states is held responsible for the white-light emission.



If the observed white-light emission would be true blackbody emission and the detector would have a constant sensitivity over the whole spectral range, the measured signal intensity would be proportional to the temperature of the sample to the fourth power (Stefan–Boltzmann law). With a wavelength-dependent sensitivity of the detection system given by  $f(\lambda)$ , and a (time-dependent) density of states of the blackbody at temperature  $T$  given by  $\rho(T(t), \lambda)$  the time-dependent signal intensity  $S(t, T)$  is given by:

$$S(t, T) = \int f(\lambda) \rho(T(t), \lambda) d\lambda. \quad (1)$$

Taking, for instance,  $f(\lambda)$  from the data sheets of the photodiode and the MCT detector, together with the filters used, leads to dependencies of the signal intensity as a function of (constant) temperature as shown in Fig. 5. In the inset of the figure the blackbody emission spectrum as would be recorded with the photodiode is shown for various temperatures.

It is evident from (1) as well as from Fig. 5 that the signal intensity depends, especially in the case when the Si photodiode used to measure the emission, highly nonlinearly on temperature. In return, an observed nonlinear signal response as a function of laser power or time, does therefore not necessarily imply that the temperature of the sample varies nonlinearly with either variable. It is therefore desirable to convert the profiles of intensity vs. time in Fig. 3a to profiles of temperature vs. time. This can be done using the curves in Fig. 5. However, two factors complicate this procedure. First, the signals of both detectors are recorded on a relative scale and two unknown scaling factors connect the curves in Figs. 3a and 5. A further possible complication is that (1) assumes, that only the spectral distribution of the sample changes and that the number of sites emitting light remains constant. In case the number of sites changes in time, the ratio of the signals from both detectors can be used to determine the temperature as a function of time. A useful check on whether the

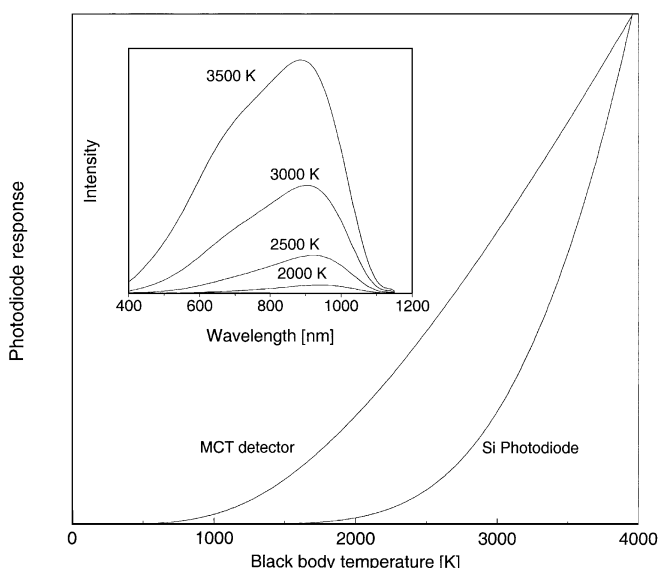


**Fig. 5.** Signal intensity of a photodiode as a function of blackbody temperature and of a MCT detector with sapphire and germanium window, as employed in the experiment. In the inset, the argument of the integral in (1) in the case of the Si photodiode is shown for various temperatures

number of sites changes is to examine the ratio of the signal from the Si and MCT detector as a function of the signal level of the Si detector (or MCT detector). When this ratio is different for the same signal levels on the left and the right side of a peak in Fig. 2, the number of sites changes in time. Otherwise, the number of sites most likely remains constant. For low excitation fluences such as used in Fig. 3a, it is found that this ratio is independent of whether one is in the rising (heating) part of the curve or the falling (cooling) part. We can therefore safely assume that the number of sites emitting light stays roughly constant during and after an IR excitation pulse.

Both curves in Fig. 3a are therefore separately converted to a temperature and the result is shown in Fig. 6. As the absolute signal level is not known, the conversion is done for three different maximum temperatures (2000, 3000 and 4000 K). Conversion of the curves of the two detectors results in only slightly different temperature vs. time curves and their averages are shown. It should be noted that, in principle, the maximum temperature can be determined by adjusting this temperature such that the curves of both detectors match. In practice however, this approach failed, presumably because Fig. 5 does not reproduce the sensitivity of the two detectors and the white-light emission is only approximately blackbody emission. In the lower part of Fig. 6 the envelope of the FELIX micropulses is shown, together with the time-integrated FELIX intensity. Neither of the curves shown in the upper part of the figure shows a strongly nonlinear rise in temperature during the FELIX pulse, nor do they show a strongly nonlinear decay after the FELIX pulse is over.

All curves actually rise slower than the time-integrated FELIX intensity. This seems to indicate that sequential single-photon absorption per micropulse linearly increases the temperature of the emitting sample with time, but is competing with heat-loss channels. For internally hot  $C_{60}$  molecules in the gas phase, cooling can occur via thermionic emission of electrons, loss of  $C_2$  fragments, and/or radiative cooling [20]. In the solid, additional heat-loss due to conduction can take place. The combination of the absorption

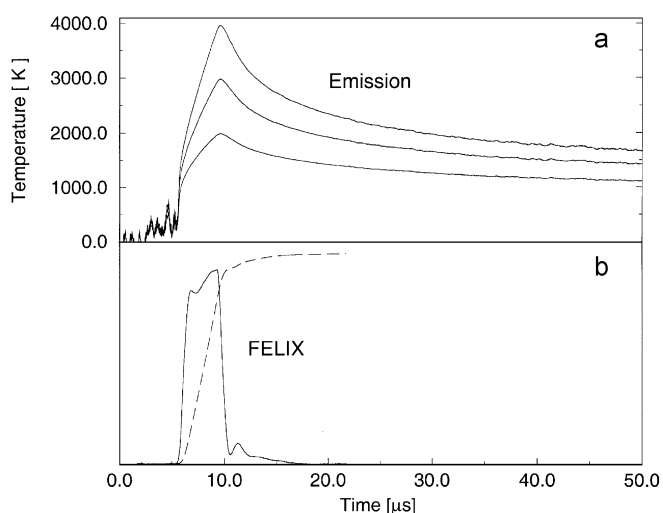


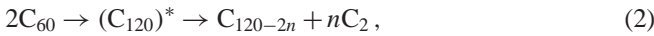
**Fig. 6.** **a** Temperature dependence of the emitting blackbody as a function of time, as obtained by converting the observed white-light emission intensity (Fig. 3a) to a temperature, using the conversion curve shown in Fig. 5. **b** Envelope of the micropulses used in recording the data displayed in **a** and its integral (dashed line)

together with these heat loss channels will result in a complicated expression for the time dependence of the temperature.

An unusual observation is the production of  $C_{60}^+$  ions, even without the presence of fragment ions such as  $C_{58}^+$ . In order to ionize gas-phase  $C_{60}$  molecules with the same infrared laser, fluences of  $\approx 300 \text{ J/cm}^2$  are needed on resonance [21], whereas with an (off-resonant)  $\text{CO}_2$  laser an order of magnitude higher fluence is needed [22]. Fluences in the present experiment are always less than  $0.1 \text{ J/cm}^2$ , nonetheless,  $C_{60}^+$  ions are observed. The ionization potential (IP) of  $C_{60}$  is around  $7.6 \text{ eV}$  [23]. For direct multiphoton ionization, absorption of more than 60 photons of  $1000 \text{ cm}^{-1}$  is needed. Moreover, a direct multiphoton ionization is unlikely because of fast internal energy redistribution.

Another possibility of obtaining  $C_{60}$  ions is via thermionic emission of electrons. Gas-phase  $C_{60}$  molecules that are internally excited are known to auto-ionize and this thermionic emission process can be faster than fragmentation. For this process to be observable in our experimental time window, internal temperatures of the  $C_{60}$  molecules above  $3000 \text{ K}$  are needed [17]. With a vibrational heat capacity of  $0.0138 \text{ eV/K}$  [24], this results in a required internal energy per  $C_{60}$  molecule of more than  $40 \text{ eV}$ . A typical laser fluence in our experiment is  $20 \text{ mJ/cm}^2$ . The required absorption cross section for a  $C_{60}$  molecule to acquire  $40 \text{ eV}$  is therefore  $3.2 \times 10^{-16} \text{ cm}^2$  – orders of magnitude higher than typical vibrational (infrared) transitions in molecules.

In the experiment, not only  $C_{60}^+$  ions are observed but also larger ions such as, for example,  $C_{120}^+$  and  $C_{180}^+$ . Ions in this size range have been observed by other groups, albeit under different experimental conditions [19]. We attribute these observations to the coalescence of  $C_{60}$  molecules to form larger fullerenes. The previously observed coalescence of two  $C_{60}$  molecules has been attributed to the following gas-phase mechanism [19]:



where the above product can then react further with  $C_{60}$  to form larger coalescence products. The coalescence product is generated internally hot and cools itself through evaporation of  $C_2$  units. Reaction products with more than 120 atoms are then generated by a reaction of the above reaction product with free  $C_2$  fragments (or by further reaction with  $C_{60}$  to give rise to peaks in the region around  $C_{180}$ ). Since the  $C_2$  supply is limited, distributions are expected and observed always to be peaked below  $n \times 60$  ( $n = 2, 3 \dots$ ) atoms [19]. In contrast, in the mass spectrum as shown in Fig. 4, the distributions peaks at masses above  $n \times 60$  ( $n = 2, 3 \dots$ ) atoms. A possible explanation is that we do observe coalescence that takes place in the solid and different distributions might result.

There are at least two possibilities for transferring a large amount of energy to  $C_{60}$  molecules: either strongly absorbing species (contaminations) that are present in low concentrations or a large amount of weakly absorbing species being present that absorb light throughout the crystal and then pool the energy together. In both cases, a dependence of the white-light or ion emission with excitation wavelength as in Fig. 1 can result since only photons that are not absorbed by regular  $C_{60}$  modes can contribute.  $C_{60}$  therefore acts like a filter resulting in the least signal when  $C_{60}$  absorbs the most. A possible example of the ‘weak absorber’ scenario might be multi-

photon absorption to the electronically excited triplet state (or absorption to the lowest singlet state followed by fast internal conversion to the triplet state). Those triplet excitations are known to be long-lived and able to diffuse through solid  $C_{60}$  [26]. After some time, they could get trapped at some defect sites where a high energy density could be obtained. The lowest excited states for  $C_{60}$  in the solid are a singlet state (S1) at  $13\,631 \text{ cm}^{-1}$  [25] and a triplet state (T1) state at  $11\,600 \text{ cm}^{-1}$  [26]. More than ten photons are needed to access these states and we would expect a high power dependence in the absorption step. Further, for such a mechanism to be applicable to our experiment, the excited-state lifetime has to be on the order of  $\mu\text{s}$  and the excitation has to be able to travel distances of up to mm. It seems therefore unlikely that such a process is responsible for our observations.

The other possibility is the presence of very dilute highly absorbing species. Those species might absorb single photons sequentially and the resulting signal could show a only a weak (linear) dependence on peak power. Upon photon absorption, the absorbing species and their vicinity thermally heat up so that fullerene coalescence can be initiated. As we discussed above, the cross section for those sites needs to be larger than  $3.2 \times 10^{-16} \text{ cm}^2$  and vibrational transitions can be excluded. Electronic transitions on the other hand, can be much stronger than vibrational transitions. In the infrared, electronic transitions can only be achieved in semiconductors or metals. Interestingly, in the mass spectra shown in Fig. 4, large amounts of potassium ions are observed. Fullerene crystals intercalated with metal atoms have been studied by solid-state chemists and physicists for a number of years [2–4]. For many metal atoms, those species are highly stable and form easily. In the case of intercalation with alkali metals, the metal atom can donate its valence electron to a  $C_{60}$  molecule. The sample can then behave metallic-like [4] with the electron being delocalized over several  $C_{60}$  molecules. Those sites could then strongly absorb the IR light in an electronic transition. In addition, it is known that  $A_1C_{60}$  [4] ( $A=\text{K}$  or other alkali metals) can have polymeric phases in which  $C_{60}$  molecules are linked by chemical bonds and this ‘polymeric’ form of  $A_1C_{60}$  could be an ideal precursor to coalescence.

It is therefore possible that small impurities of alkali atoms in the lattice of our  $C_{60}$  molecules are responsible for the processes observed. These impurities might be either introduced during the production process or sputtered off the substrate on which  $C_{60}$  is resting by the IR laser. This explains the observation that on fresh crystals, light emission is predominantly observed from the bottom of the crystal. Upon turning the crystal around, emission occurs from the top layers in localized spots. By donating an electron, the alkali atom activates the chromophore, which then strongly absorbs IR light. When the internal energy is high enough, coalescence of fullerenes starts and thermal blackbody radiation as well as ion emission is observed. During that process, the alkali atom might either be ejected as well or travel deeper in the crystal to activate other sites. We think that the above mechanism provides a plausible explanation for the observations we made. At this point, we can only speculate whether this mechanism is also applicable to the results by Roth and coworkers [8–10], where visible laser radiation is used. However, their interpretations of the origin of the light emission are based on an emission spectrum that is apparently not corrected for detector response and on a power and decay be-

havior that is not corrected for the emission characteristics (i.e. blackbody) of the sample. We therefore feel that the data and interpretation shown here might present an alternative explanation for their results as well.

#### 4 Conclusions

The interaction of  $C_{60}$  with tunable and pulsed IR radiation has been studied. At specific wavelengths white-light emission as well as emission of ionic species from the crystal is observed. These processes occur at wavelengths where  $C_{60}$  is relatively transparent and we can conclude that regular  $C_{60}$  is not the chromophore for light absorption. The white-light emission follows a blackbody curve which complicates the interpretation of its dependence on excitation power as well as its temporal evolution. It is concluded that the absorption process has a power dependence that is close to linear and that the chromophore has to be a strong absorber that is present only in a very dilute form in the crystal. Plausible absorbers are sites that are intercalated with alkali metal ions.

*Acknowledgements.* We gratefully acknowledge the support by the 'Stichting voor Fundamenteel Onderzoek der Materie' (FOM) in providing the required beam time on FELIX and highly appreciate the skillful assistance by the FELIX staff, in particular Dr. A.F.G. van der Meer. We would like to thank Dr. Richard Engeln for help in the dispersed emission measurements. This work has become possible by financial support by the Netherlands Organization for Scientific Research (NWO) via PIONIER-grant # 030-66-89.

#### References

1. J.E. Fischer, P.A. Heiney: *J. Phys. Chem. Solids* **54**, 1725 (1993)
2. A.F. Hebard, M.J. Rosseinsky, R.C. Haddon, D.W. Murphy, S.H. Glarum, T.T.M. Palstra, A.P. Ramirez, A.R. Kortan: *Nature* **350**, 600 (1991)
3. J. Winter, H. Kuzmany: *Solid State Commun.* **84**, 935 (1992)
4. O. Chauvet, G. Oszlanyi, L. Forro, P.W. Stephens, M. Tegze, G. Faigel, A. Janossy: *Phys. Rev. Lett.* **72**, 2721 (1994)
5. A.M. Rao, P. Zhou, K.A. Wang, G.T. Hager, J.M. Holden, Y. Wang, W.T. Lee, X.X. Bi, P.C. Eklund, D.S. Cornett, M.A. Duncan, I.J. Amster: *Science* **259**, 955 (1993)
6. P. Zhou, A.M. Rao, K.A. Wang, J.D. Robertson, C. Eloi, M.S. Meier, S.L. Ren, X.X. Bi, P.C. Eklund, M.S. Dresselhaus: *Appl. Phys. Lett.* **60**, 2871 (1992)
7. J. Feldmann, R. Fischer, W. Guss, E.O. Göbel, S. Schmitt-Rink, W. Krätschmer: *Europhys. Lett.* **20**, 553 (1992)
8. H.J. Byrne, W.K. Maser, W.W. Rühle, A. Mittelbach, S. Roth: *Appl. Phys. A* **56**, 235 (1993); H.J. Byrne, W.K. Maser, W.W. Rühle, L. Akselrod, A.T. Werner, J. Anders, X.Q. Zhou, G. Mahler, T. Kuhn, A. Mittelbach, S. Roth: *Appl. Phys. A* **57**, 303 (1993); H.J. Byrne, W.K. Maser, K. Kaiser, L. Akselrod, J. Anders, W.W. Rühle, X.Q. Zhou, A. Mittelbach, S. Roth: *Appl. Phys. A* **57**, 81 (1993); H.J. Byrne, W.K. Maser, W.W. Rühle, A. Mittelbach, W. Hönl, H.G. von Schnering, B. Movaghar, S. Roth: *Chem. Phys. Lett.* **203**, 461 (1993)
9. A.T. Werner, H.J. Byrne, S. Roth: *Full. Sci. Tech.* **4**, 757 (1996)
10. A.T. Werner, J. Anders, H.J. Byrne, W.K. Maser, K. Kaiser, A. Mittelbach, S. Roth: *Appl. Phys. A* **57**, 157 (1993)
11. T.T.M. Palstra, R.C. Haddon, K.B. Lyons: *Carbon* **35**, 1825 (1997)
12. D. Oepts, A.F.G. van der Meer, P.W. van Amersfoort: *Infrared Phys. Technol.* **36**, 297 (1995)
13. G.M.H. Knippels, R.F.X.A.M. Mols, A.F.G. van der Meer, D. Oepts, P.W. van Amersfoort: *Phys. Rev. Lett.* **75**, 1755 (1995)
14. M.A. Verheijen, W.J.P. van Enckevort, G. Meijer: *Chem. Phys. Lett.* **216**, 72 (1993)
15. S. Leach, M. Vervloet, A. Despres, E. Breheret, J.P. Hare, T.J. Dennis, H.W. Kroto, R. Taylor, D.R.M. Walton: *Chem. Phys.* **160**, 451 (1992)
16. W. Krätschmer, L.D. Lamb, K. Fostiropoulos, D.R. Huffman: *Nature* **347**, 354 (1990)
17. E.E.B. Campbell, G. Ulmer, I.V. Hertel: *Phys. Rev. Lett.* **67**, 1986 (1991)
18. P. Wurz, K.R. Lykke: *J. Chem. Phys.* **95**, 7008 (1991)
19. C. Yertzian, K. Hansen, F. Diederich, R.L. Whetten: *Nature* **359**, 44 (1992); R.D. Beck, P. Weis, G. Bräuchle, M.M. Kappes: *J. Chem. Phys.* **100**, 262 (1994); K. Hansen, C. Yertzian, R.L. Whetten: *Chem. Phys. Lett.* **218**, 462 (1994)
20. R. Mitzner, E.E.B. Campbell: *J. Chem. Phys.* **103**, 2445 (1995)
21. G. von Helden, I. Holleman, G.M.H. Knippels, A.F.G. van der Meer, G. Meijer: *Phys. Rev. Lett.* **79**, 5234 (1997)
22. M. Hippler, M. Quack, R. Schwarz, G. Seyfang, S. Matt, T. Märk: *Chem. Phys. Lett.* **278**, 111 (1997)
23. P. Scheier, B. Dünser, R. Wörgötter, M. Lezius, R. Robl, T.D. Märk: *Int. J. Mass Spectrom. Ion Processes* **138**, 77 (1994)
24. E. Kolodney, A. Budrevich, B. Tsipinyuk: *Phys. Rev. Lett.* **74**, 510 (1995)
25. D.J. van den Heuvel, G.J.B. van den Berg, E.J.J. Groenen, J. Schmidt, I. Holleman, G. Meijer: *J. Phys. Chem.* **99**, 11644 (1995)
26. D.J. van den Heuvel, I.Y. Chan, E.J.J. Groenen, J. Schmidt: *Chem. Phys. Lett.* **231**, 111 (1994)